

Article

LEDCNet: A Lightweight and Efficient Semantic Segmentation Algorithm Using Dual Context Module for Extracting Buildings and Roads from UAV Aerial Remote Sensing Images

Xiaoxiang Han ^{1,†}, Yiman Liu ^{3,4,†}, Gang Liu ⁵, Yuanjie Lin ¹ and Qiaohong Liu ^{2,*}

- ¹ School of Health Sciences and Engineering, University of Shanghai for Science and Technology, Shanghai 200093, China; gtlinyer@163.com (X.Han.); linyuanjie0312@163.com (Y.Lin.)
- ² School of Medical Instruments, Shanghai University of Medicine and Health Sciences, Shanghai 201318, China; hqllqh@163.com (Q.Liu.)
- ³ Department of Pediatric Cardiology, Shanghai Children's Medical Center, School of Medicine, Shanghai Jiao Tong University, Shanghai 200127, China; LiuyimanSCMC@163.com (Y.Liu.)
- ⁴ Shanghai Key Laboratory of Multidimensional Information Processing, School of Communication & Electronic Engineering, East China Normal University, Shanghai 200241, China
- ⁵ Key Laboratory of Earthquake Geodesy, Institute of Seismology, China Earthquake Administration, Wuhan 430071, China; whgpslg@gmail.com (G.Liu.)
- * Correspondence: hqllqh@163.com; Tel.: +86-137-6183-3680
- † These authors contributed equally to this work.

Abstract: Semantic segmentation for extracting buildings and roads, from unmanned aerial vehicle (UAV) remote sensing images by deep learning becomes a more efficient and convenient method than traditional manual segmentation in surveying and mapping field. In order to make the model lightweight and improve the model accuracy, A Lightweight and Efficient Network implemented using Dual Context modules (LEDCNet) for Buildings and Roads from UAV Aerial Remote Sensing Images is proposed. The proposed network adopts an encoder-decoder architecture in which a Lightweight Densely Connected Network (LDCNet) is developed as the encoder. In the decoder part, the dual multi-scale context modules which consist of the Atrous Spatial Pyramid Pooling module (ASPP) and the Object Contextual Representation module (OCR) are designed to capture more context information from feature maps of UAV remote sensing images. Between ASPP and OCR, a Feature Pyramid Network (FPN) module is used to and fuse multi-scale features extracting from ASPP. A private dataset of remote sensing images taken by UAV which contains 2431 training sets, 945 validation sets, and 475 test sets is constructed. The proposed model performs well on this dataset, with only 1.4M parameters and 5.48G floating-point operations (FLOPs), achieving an mean intersection-over-union ratio (mIoU) of 71.12%. More extensive experiments on the public LoveDA dataset and CITY-OSM dataset to further verify the effectiveness of the proposed model with excellent results on mIoU of 65.27% and 74.39%, respectively.

Keywords: Remote Sensing, Semantic Segmentation, Context Features, Lightweight Network

Citation: Han, X.; Liu, Y.; Lin, Y.; Liu, Q. LEDCNet: A Lightweight and Efficient Semantic Segmentation Algorithm Using Dual Context Module for Extracting Buildings and Roads from UAV Aerial Remote Sensing Images. *Drones* **2023**, *1*, 0. <https://doi.org/>

Received:

Revised:

Accepted:

Published:

Copyright: © 2023 by the authors. Submitted to *Drones* for possible open access publication under the terms and conditions of the Creative Commons Attribution (CC BY) license (<https://creativecommons.org/licenses/by/4.0/>).

1. Introduction

Unmanned aerial vehicle (UAV) with some advantages, such as less susceptible to atmospheric interference, low flight altitude, high resolution and, low operating costs[1] has been widely used in land surveying and mapping, ecological environment monitoring, resource survey and classification etc.. Compared with other aerial photography collection methods, the high resolution remote sensing images taken by UAV is more suitable to extract various important ground objects, e.g., building and road.

In recent years, with the rapid development of deep learning, models based on convolutional neural networks have shown superior performance in some computer vision tasks such as image classification, detection, and segmentation, etc.. Compared with traditional machine learning algorithms with manual features extraction, deep learning can automatically extract features including color, texture, shape and spatial position relationship of the image. Fully Convolutional Network (FCN)[2], as the first semantic segmentation of natural images only using convolutional operation, realized the pixel level classification of the images. Then, there are more semantic segmentation models[3–9] significantly improved the segmentation performance. All of these algorithms predict the pixel level labels based on the semantic information represented by image pixels. Recently, some new deep learning methods have been proposed for extracting buildings or roads from UAV remote sensing images. Liu et al.[10] introduced a chain-based U-Net network to address the problem of incomplete building boundary extraction. Hossain et al.[11] proposed a hybrid image segmentation method that achieved better results in building extraction. Additionally, Sulstonov et al.[12] designed a lightweight hybrid method based on U-Net for road extraction. Guan et al.[13] proposed an attentive capsule feature pyramid network for UAV image road extraction. However, these methods can only extract buildings or roads separately. Therefore, a lightweight network is needed that can simultaneously extract buildings and roads from UAV images.

Different from natural images, UAV remote sensing images are often very large in size, usually with a resolution of tens of thousands by tens of thousands. UAV remote sensing image segmentation is a challenging task due to the large variations in the size, shape, color and location of the ground object, as shown in Fig.1.. Figs. 1a and 1d show the different style buildings though they belong to the same ground object. In the other case, the surface feature elements of different ground objects may be similar. As shown in Figs. 1b and 1e, the top of a concrete building is very similar to the surface of a concrete road, leading to difficulty in feature extraction.

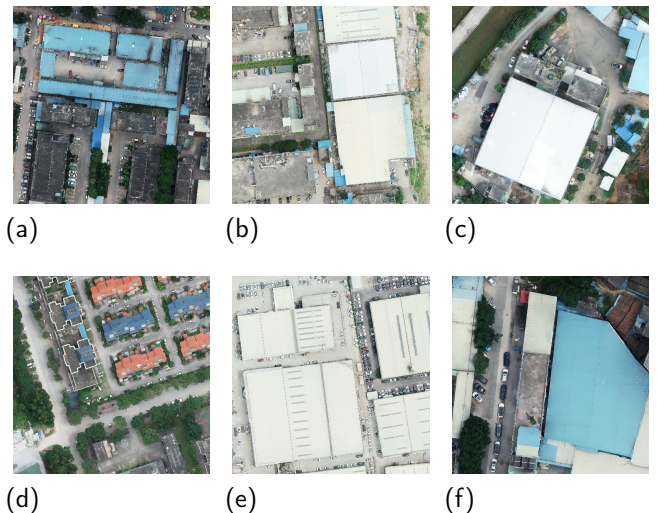


Figure 1. Some examples from our private dataset.

A lot of greenery on both sides or in the center of the road, and vehicles on the road cover the road, which would affect the road surface segmentation results, as shown in Figs. 1c and 1f. In addition, buildings with different scales are likely to affect the performance of the model, which requires the model with a strong ability to extract multi-scale context features.

To address these issues, a new deep neural network structure, called LEDCNet, is proposed for the extraction of buildings and roads from UAV remote sensing images. While DenseNet[14] has strong feature extraction ability, its parameters and calculations are large. Moreover, Liu et al.[15] developed a convolutional neural network (CNN) called ConvNeXt, which obtained a superior performance beyond Swin Transformer[16] by improving ResNet[17]. Inspired by this, we propose a lightweight, high-performance convolutional neural network named LDCNet, which serves as the backbone structure of LEDCNet for semantic segmentation of remote sensing images. Our goal is to extend LDCNet to become a new generation backbone network for lightweight semantic segmentation algorithms. LEDCNet is an encoder-decoder

structure that employs LDCNet as the encoder, which has demonstrated excellent segmentation results. In the decoder, we introduce dual context feature extraction modules, which combine the Atrous Spatial Pyramid Pooling (ASPP) module[8] and the Object Context Representation (OCR) module[18]. The Feature Pyramid Network (FPN)[19] module is used to fuse multi-scale features after the ASPP operation and before the OCR operation.

The main contributions of this paper are as follows.

1. A new network based on encoder-decoder structure for the extraction of feature elements from UAV remote sensing images is proposed. A new LDCNet that is proposed in this paper is employed as a lightweight encoder to reduce model's parameters and accelerate the computational speed. And a dual multi-scale contextual feature extraction module combines with the ASPP and OCR is used to as an effective decoder to fuse and refine the target objects and boundary features;
2. A lightweight and high-performance backbone network called LDCNet, which uses the design ideas of ConvNeXt and DenseNet is developed. The LDCNet is an efficient light-weight network for features extraction of UAV remote sensing images with fewer parameters;
3. Extensive experiments are carried out to verify the effectiveness and feasibility of the proposed method on our private database and two publicly datasets, i.e., LoveDA and CITY-OSM. Several most popular backbone networks and semantic segmentation algorithms are used to compared with the proposed method on the semantic segmentation of UAV remote sensing images. The experimental results show that the proposed method can effectively extract the road and building with higher accuracy than the other compared networks.

2. Related Works

2.1. Semantic Segmentation in Remote Sensing

Fully convolutional networks (FCN), as the first semantic segmentation network based on deep learning, can accept the input size of any size. To segment the remote sensing images with more complex, there are some improved FCN-based networks proposed to enhance the segmentation performance. Maggiori et al.[20] designed a dual-scale neuron module based on FCN for semantic segmentation of remote sensing images, which balances the accuracy of recognition and localization. Liu et al.[21] proposed an improved FCN to high-resolution remote sensing image segmentation. However, FCN has limited ability to extract objects of very small size or very large size[2]. Fu et al.[22] adopted dilated Atrous convolution to optimize the FCN model and used conditional random field (CRF) to post-process preliminary segmentation results, which result in a significant improvement over previous networks. Atrous convolution can increase the receptive field of the convolution while maintaining the spatial resolution of the feature map.

U-Net[4] is another popular semantic segmentation network, which was first used in medical image segmentation. Li et al.[23] proposed a network to segment the land and sea of high-resolution remote sensing images based on U-Net. Cheng et al.[24] developed a network called HDCUNet combining U-Net with Hybrid Dilated Convolution (HDC) for fast and accurate extraction of coastal farming areas. It avoids meshing and increases the receptive field. Wang et al. [25] designed a U-Net with two decoders and introduced spatial attention and channel attention.

In addition, some researches[3,26] improved SegNet[3] for semantic segmentation of remote sensing images. Weng et al.[27] proposed an SR-SegNet using a separable residual algorithm for water extraction from remote sensing images. Kniaz et al.[28] developed a network called GeoGAN based on the Generative Adversarial Network (GAN)[29] to extract waters in different seasons. Recently, some Transformer-based or the combination of Transformer and

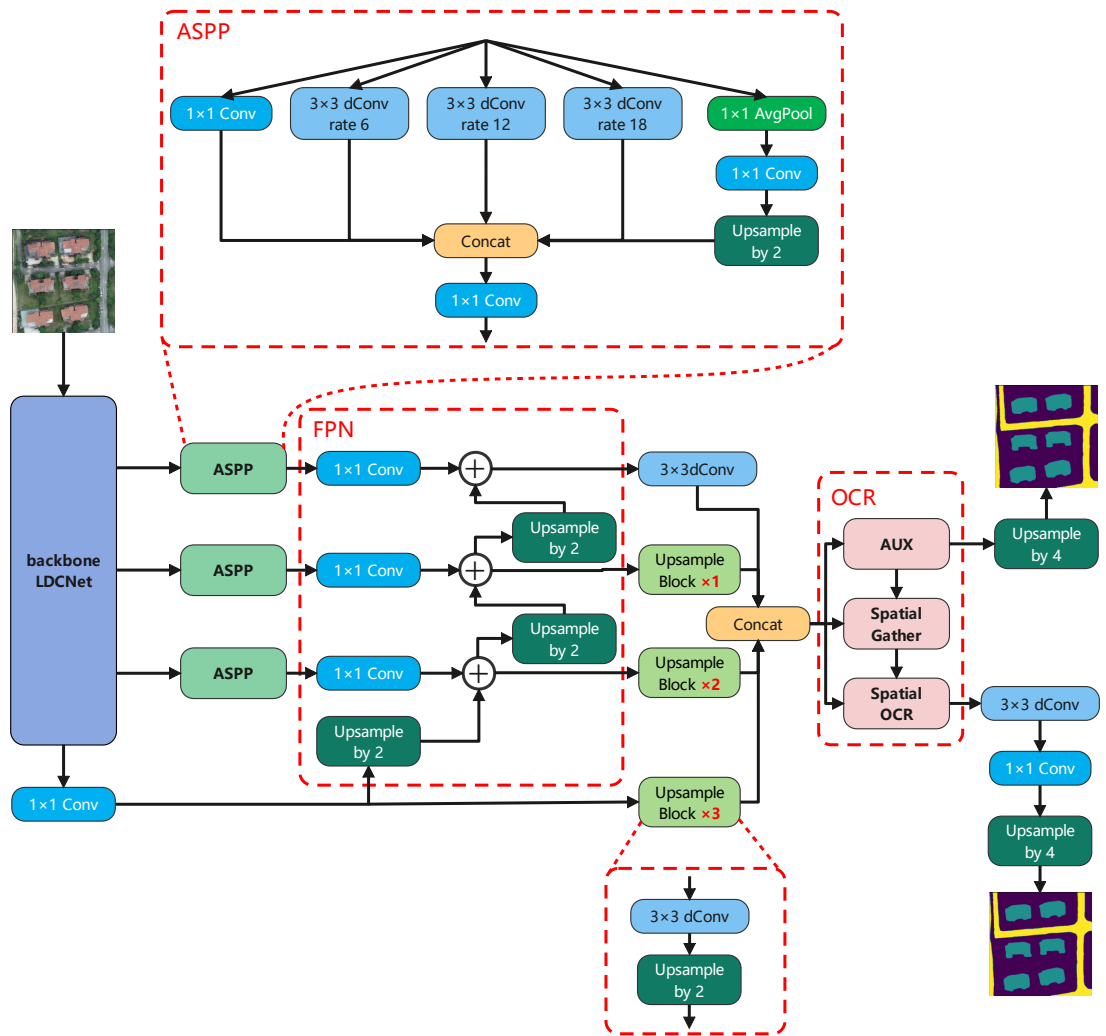


Figure 2. The overall architecture of LEDCNet, and the details of ASPP.

CNN models[30–32] promoted the semantic segmentation performance with the Transformer’ advantage of global receptive field. However, the large parameters of Transformer affects the calculation speed of these proposed models.

2.2. Lightweight Network

In order to deploy the network models on devices with limited resources, it is necessary to design lightweight and efficient networks. The MobileNet series[33–35] is a classic lightweight network that applies depthwise separable convolutions[33], inverted residuals[34], linear bottlenecks[34], and lightweight channel attention modules[35]. It can achieve higher accuracy with fewer parameters and lower calculation costs. SqueezeNet[36], another lightweight network, used the Fire module for parameter compression. EffectionNet[37] balanced the three dimensions of depth, width, and resolution well, and scales these three dimensions uniformly through a set of fixed scaling factors. GhostNet[38] obtains redundant information by designing cost-efficient, which ensures the model can fully understand the input data. MicroNet[39] used Micro-Factorized convolution and Dynamic Shift-Max to reduce the amount of calculation and improve network performance.

2.3. Context Feature Extraction

By fully considering the context information can significantly boost the semantic segmentation performance and solve the problem of receptive field scale. To aggregate multi-scale contextual features, PSPNet[5] used a pyramid pooling module, which connects four global pooling layers of different sizes in parallel, pools the original feature maps to generate feature maps of different levels, and restores them to the original size after convolution and upsampling. DeepLabV3[8] introduced the Atrous spatial pyramid pooling (ASPP) module, which utilized different hole rates to construct convolution kernels of different receptive fields to obtain multi-scale context information. GCNet[40] employed a self-attention mechanism to obtain global context information. GCN[41] enlarged the receptive field by increasing the size of the convolution kernel. The convolution kernel up to 15×15 in size in GCN proved that the large convolution kernel has a stronger ability to extract context features.

3. Proposed Method

3.1. Overall structure of LEDCNet

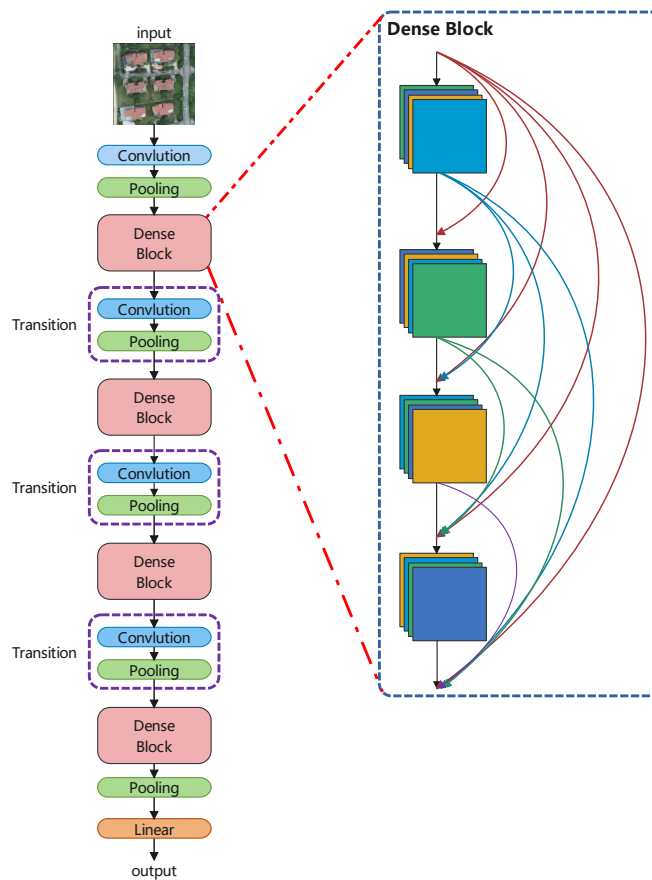


Figure 3. The overall structure and densely connected blocks of LEDCNet.

result and a feature map with object context information. This rough segmentation result is taken as one of the outputs of the network, and the feature maps are fed into the next step for further processing. Then, the feature map is processed by a refinement classification head to refine the segmentation edges. It consists of a 3×3 depthwise separable convolution and a 1×1 convolution. Finally, the feature map is upsampled to the size of the input image.

The proposed lightweight and efficient semantic segmentation network, referred to as LEDCNet, is shown in Fig.2. The proposed LEDCNet is an encoder-decoder structure. In the encoder part, LEDCNet takes our proposed LDCNet as a backbone, which can reduce model parameters and accelerate the computational speed. First, an image of size 512×512 is input into the backbone network LDCNet. And after feature extraction operation by LDCNet, four different levels of feature maps are output. The first three feature maps are respectively input into the Atrous spatial pyramid pooling module (ASPP)[8] to extract multi-scale context information. The three outputs are fed into the corresponding 1×1 convolution operation in the Feature Pyramid Network (FPN)[19] and upsampled to the same size. Four feature maps of the same size are then concatenated as the input of Object-Contextual Representation (OCR)[18] module. After the feature map is processed by OCR, it will produce a rough segmentation

3.2. LDCNet

Inspired by ConvNeXt and DenseNet, this paper develops a backbone network, called LDCNet. The structure and densely connected blocks are shown in Fig.4. ConvNeXt improved the classical ResNet by introducing some of the latest ideas and technologies of Transformer network to enhance the performance of CNN. Macro design, reference of ResNeXt's design ideas[42], inverted bottleneck layer, large convolution kernel and micro design of various layers are the five main optimization design of ConvNeXt. In the macro design of ConvNeXt, the stacking ratio of multi-stage blocks is 1:1:3:1. The number of blocks stacked in the third stage is larger. This improves the model accuracy of ConvNeXt. Following the design, we set the stacking ratio of blocks in each stage of LDCNet to 1:1:3:1. The specific layers of each stage are 2, 2, 6 and 2 respectively. The structure of the proposed LDCNet is shown in Fig.3.

ConvNeXt designs the effective inverted bottlenecks block with a 3×3 depthwise separable convolution, shown in Figs.4(a) and (b). This structure can partially reduce the parameter scale of the model while slightly improving the accuracy rate. Considering the multi-scale feature extraction ability of Inception block in GoogLeNet[43], a new bottleneck layer with two branches is proposed in this paper. One of the branches is a depthwise separable convolution with a 7×7 convolution kernel, and the other is a depthwise separable convolution with a 3×3 convolution kernel. After adding the output feature maps of two branches, and then concatenating with the input feature map, the output feature map of the proposed bottleneck layer is produced, as shown in Fig.4(c). In recent years, some new studies[41,44,45] have stated the large convolution kernels are more efficient for enlarging the receptive field. In order to obtain a higher computational efficiency, a 7×7 convolution kernel is used at the beginning of one branch in the proposed bottleneck layer.

As we all know, Batch normalization (BN)[46] is most popular optimization process in computer vision tasks by computing the mean and variance of each minibatch and pulls it back to a standard normal distribution with mean 0 and variance 1 to make neural network training faster and stabler However, BN also has may some drawbacks detrimental to the model performance[47]. Transformers use a simpler layer normalization (LN)[48], which is more common in natural language processing tasks. ConvNeXt replaces all BNs with LNs to improve the model performance. Since the features of our remote sensing images depend on the statistical parameters between different samples. it is inappropriate to replaces all BNs with LNs in the task of extracting buildings and roads from UAV remote sensing images. Therefore, we use an LN after a 3×3 depthwise separable convolution in the bottleneck layer, and replaced the BN in the transition layer with LN.

3.3. Atrous Space Pyramid Pooling (ASPP)

In order to obtain a large receptive field without losing spatial resolution and increasing computation, ASPP uses multiple parallel dilated convolutional layers with different sampling rates. The features which are extracted for each sampling rate are further processed in separate branches and fused to generate the final result.

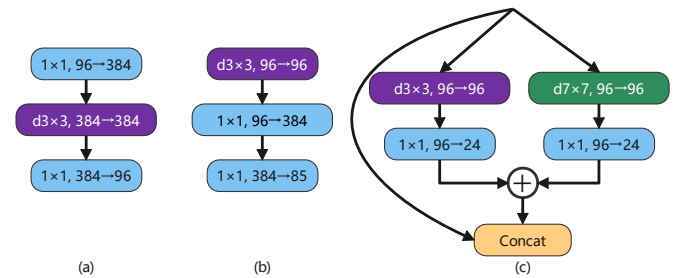


Figure 4. (a) is the inverted bottleneck layer designed by the authors of ConvNeXt. (b) is the actual bottleneck layer of ConvNeXt. (c) is our bottleneck layer for LDCNet.

Atrous convolution can expand the receptive field of the convolution kernel without loss of resolution. Using ASPP can achieve multi-scale feature extraction through different receptive fields and upsampling. In a two-dimensional convolution, for each position i on the feature y of the convolution output and the corresponding convolution kernel w , for the input x , the calculation of the dilated convolution is as follows:

$$y[i] = \sum_k x[i + r \cdot k]w[k] \quad (1)$$

where r is the hole rate, which represents the sampling step size of the convolution kernel on the input x of the convolution operation. k represents the position of the convolution kernel parameter. If the convolution kernel size is 3, then $k=0,1,2$. The receptive field of the convolution can be adaptively modified by changing the value of the dilation rate r .

3.4. Object Context Representation (OCR)

OCR considers the relationship between a pixel and its context pixels, and aggregates similar context pixel representations with higher weights. Unlike relational context method, OCR constructs contextual pixels into object regions and exploits the relationship between pixels and object regions.

The OCR module consists of three steps: soft object region extraction, object region representation computation, and object-contextual representation computation for each position. It is mainly based on the scaled dot-product self-attention of the encoder-decoder structure. The input to attention consists of: a set of N_q queries $Q \in \mathbb{R}^{d \times N_q}$, a set of N_{kv} keys $K \in \mathbb{R}^{d \times N_{kv}}$, and a set of N_{kv} values $V \in \mathbb{R}^{d \times N_{kv}}$. The attention weight a_j is computed as the Softmax normalization of the dot product between query q_i and key k_j :

$$Z_i = \sum_{j=1}^{N_{kv}} e^{\frac{1}{\sqrt{d}} q_i^\top k_j} \quad (2)$$

$$a_{ij} = \frac{e^{\frac{1}{\sqrt{d}} q_i^\top k_j}}{Z_i} \quad (3)$$

The attention output for each query q_i is the aggregation of values weighted by attention weights:

$$Attn(q_i, K, V) = \sum_{j=1}^{N_{kv}} a_{ij} V_j \quad (4)$$

For object context representation, the calculation formula of the relationship between each pixel and each object area is as follows:

$$w_{ik} = \frac{e^{\kappa(x_i, f_k)}}{\sum_{j=1}^K e^{\kappa(x_i, f_j)}} \quad (5)$$

Among them, $\kappa(x, f) = \phi(x)^\top \psi(f)$ is the denormalized relationship function, $\phi(\cdot)$ and $\psi(\cdot)$ are two transformation functions implemented by $1 \times 1 \text{Conv} \rightarrow \text{BN} \rightarrow \text{ReLU}$.

4. Experiment

4.1. Dataset

A private dataset of UAV-borne remote sensing images with a resolution between 10000×10000 and 20000×20000 is constructed. Each remote sensing image which corresponds to the red (R), green (G), and blue (B) bands is cropped to the same size of 512×512 . All the images are

divided into a training set of 2431 images, a validation set of 945 images, and a test set of 676 images. The category labels of two important ground objects, i.e., road and building, are manually annotated. The training and validation sets are from a city in Guangdong, China, and the test set is from a place along the Yangtze River, China.

Furthermore, in order to verify the competitive performance and model generalization ability of our proposed model in the task of semantic segmentation of aerial remote sensing images, we test it on two public datasets, i.e., LoveDA[49] and CITY-OSM[50]. LoveDA dataset includes the cities of Nanjing, Changzhou and Wuhan in China, with a total of 5987 high spatial resolution (0.3 m) remote sensing images, with a training set of 2522 images, a validation set of 1669 images, and a test set of 1796 images. The pixels in each image are divided into six categories, namely road, building, water, barren, forest, agricultural, and background. For the sake of fairness, we only take two types of ground objects, building and road. CITY-OSM dataset includes Berlin and Potsdam in Germany, Chicago in the United States, Paris in France, Zurich in Switzerland and Tokyo in Japan, with a total of 1641 aerial images. Its labels are two types of ground objects, i.e., building and road, which are consistent with the label categories of our private dataset. We remove the images that are obviously mislabeled in this dataset, for example the entire image is labelled as a building or a road. All the images are cropped and scaled to the size of 512×512 , which are divided into a training set of 10621 images, a validation set and a test set of 3401 images.

4.2. Training Details

We designed our model based on the machine learning framework PyTorch1.12.1 using Python3.8. In particular, we also use PyTorch-Lightning1.6.5, an efficient and convenient framework based on PyTorch. In addition, some of our comparison experiments and ablation experiments use the backbone network provided in Torchvision0.13.1.

We trained the proposed model on a GPU server with an Intel Core i9-10900X CPU, two 10GB Nvidia RTX3080 GPUs, 32GB RAM, and 20GB VRAM.

We set the batch size of data according to different networks to ensure maximum memory utilization. The number of threads of the data reading program is 16. The initial learning rate is $1e-3$. The learning rate dynamic adjustment strategy is ReduceLRonPlateau. The optimizer is AdamW[51]. The training epoch number is 100. Train with automatic mixed precision. The loss function is FocalLoss[52], which can reduce the weight of samples that are easy to classify and increase the weight of samples that are difficult to classify. Its formula is as follows:

$$FL(p_t) = -\alpha_t(1 - p_t)^\gamma \log(p_t) \quad (6)$$

$p \in [0,1]$ is the model's estimated probability of the labeled class, γ is an adjustable focusing parameter, and α is a balancing parameter. We set γ to 2 and α to 0.25.

4.3. Evaluation Metrics

In order to evaluate the performance and efficiency of the proposed LEDCNet model, our evaluation indicators are divided into two categories. The first category is to evaluate the accuracy of the network, including Overall Accuracy (OA), average F1-Score (F1) and mean Intersection over Union (mIoU). The results of these evaluation indicators are calculated based on the confusion matrix, where TP indicates the number of True Positive categories, TN indicates the number of True Negative categories, FP indicates the number of False Positive categories, and FN indicates the number of False Negative categories.

overall Accuracy (OA) is used to measure the overall accuracy of the model prediction results:

$$OA = \frac{TP + TN}{TP + TN + FP + FN} \quad (7)$$

The F1-Score (F1) indicates the comprehensive consideration of Precision and Recall:

$$Precision = \frac{TP}{TP + FP} \quad (8)$$

$$Precision = \frac{TP}{TP + FN} \quad (9)$$

$$F1 = 2 \frac{Precision \times Recall}{Precision + Recall} = \frac{2TP}{2TP + FP + FN} \quad (10)$$

Intersection over Union (IoU) is used to measure the ratio of the intersection and union of the predicted results of a certain category and the true value of the model:

$$IoU = \frac{TP}{TP + FN + FP} \quad (11)$$

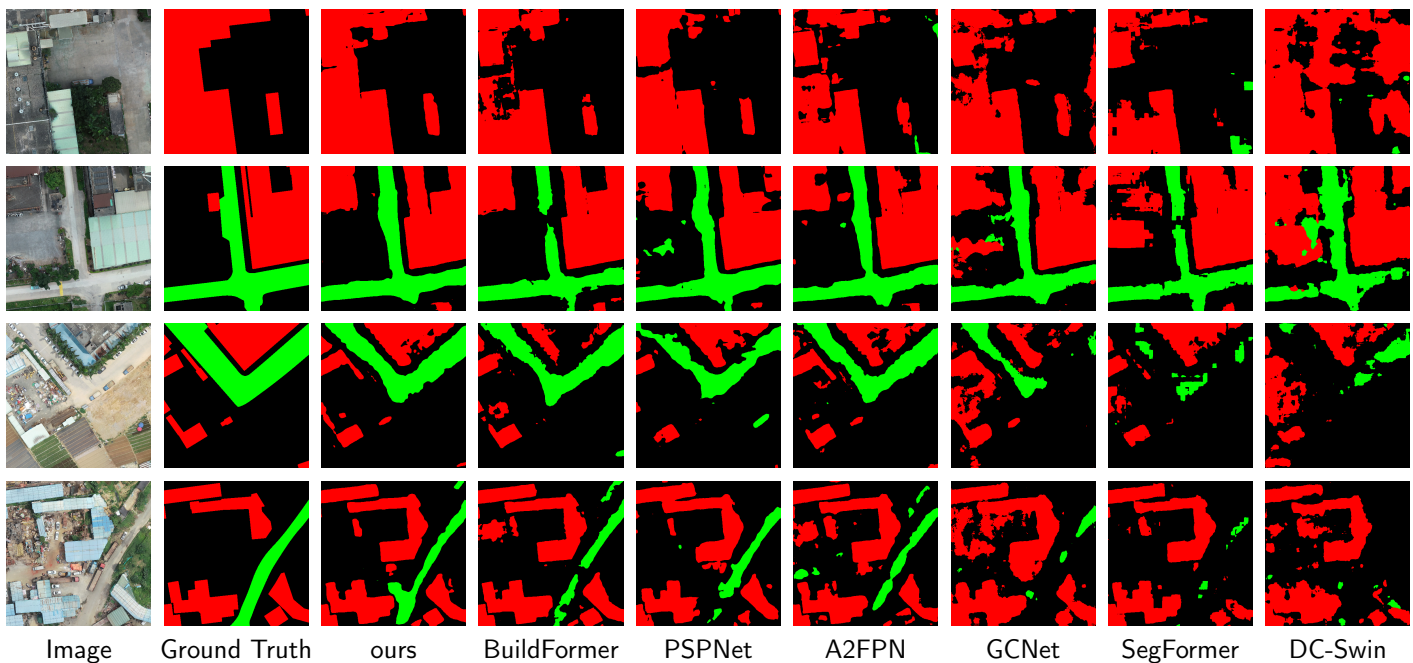
The second category is to evaluate the scale of the network, including floating point operations (FLOPs) for evaluating complexity, frames per second (FPS) for evaluating speed, memory usage (MB) and the number of model parameters (M) to evaluate memory requirements.

4.4. Experimental results on the private dataset

In this section, LEDCNet is compared with some other semantic segmentation models on the constructed private dataset. These models include GCNet[40], PSPNet[5], SegFormer[53], and A2FPN[54], DC-Swin[55], BuildFormer[56] proposed for remote sensing semantic segmentation. The backbone network of the other compared models is ResNet18, and LEDCNet uses the proposed backbone network LDCNet. LEDCNet is divided into two versions, the basic version and the large version. The only difference is that the depth of LDCNet is different. The number of dense block stacks in the basic version is 2, 2, 6, 2, while the number of stacks in the large version is 6, 6, 18, 6. From Table 1, it is clear seen that the proposed model outperforms other models in term of the numerical results. The mIoU of the proposed model is 4.59% higher than that of the powerful BuildFormer. And the IoU of the background, buildings and roads increased by 2.47%, 6.45% and 4.04% respectively compared with BuildFormer. Furthermore, the overall accuracy and mean F1 score of the proposed model are 0.94% and 3.40% higher than the powerful BuildFormer. However, the large-scale version of LEDCNet does not perform as well as the base version on our smaller-scale dataset, and it overfits. Moreover, LEDCNet using the proposed LDCNet as the backbone outperforms LEDCNet with ReseNet18 as the backbone. A comparison of the visual effects via different methods is depicted in Fig.5. It can be seen from the figure that the proposed model handles edges better than other methods. And the extracted buildings did not generate a large number of voids. It can extract relatively small roads.

Table 1. Experimental results on the private dataset.

Method	Backbone	Background (%)	building (%)	road (%)	OA (%)	mean F1 (%)	mIoU (%)
DC-Swin	-	76.47	55.74	23.17	87.08	65.44	52.14
SegFormer	-	78.55	56.94	36.23	88.37	71.24	57.24
GCNet	ResNet18	79.55	61.53	37.72	89.09	73.19	59.62
A2FPN	ResNet18	81.46	66.01	41.73	90.33	76.06	63.26
PSPNet	ResNet18	82.56	67.52	43.87	90.89	76.92	64.22
BuildFormer	-	83.26	68.56	47.76	91.34	78.95	66.53
LEDCNet (ours)	ResNet18	83.01	67.59	43.63	91.13	77.38	64.83
LEDCNet (ours)	LDCNet (ours)	85.73	75.01	52.70	92.83	82.35	71.12
LEDCNet-Large (ours)	LDCNet-Large (ours)	<u>84.76</u>	<u>72.93</u>	<u>51.81</u>	<u>92.31</u>	<u>81.45</u>	<u>69.87</u>

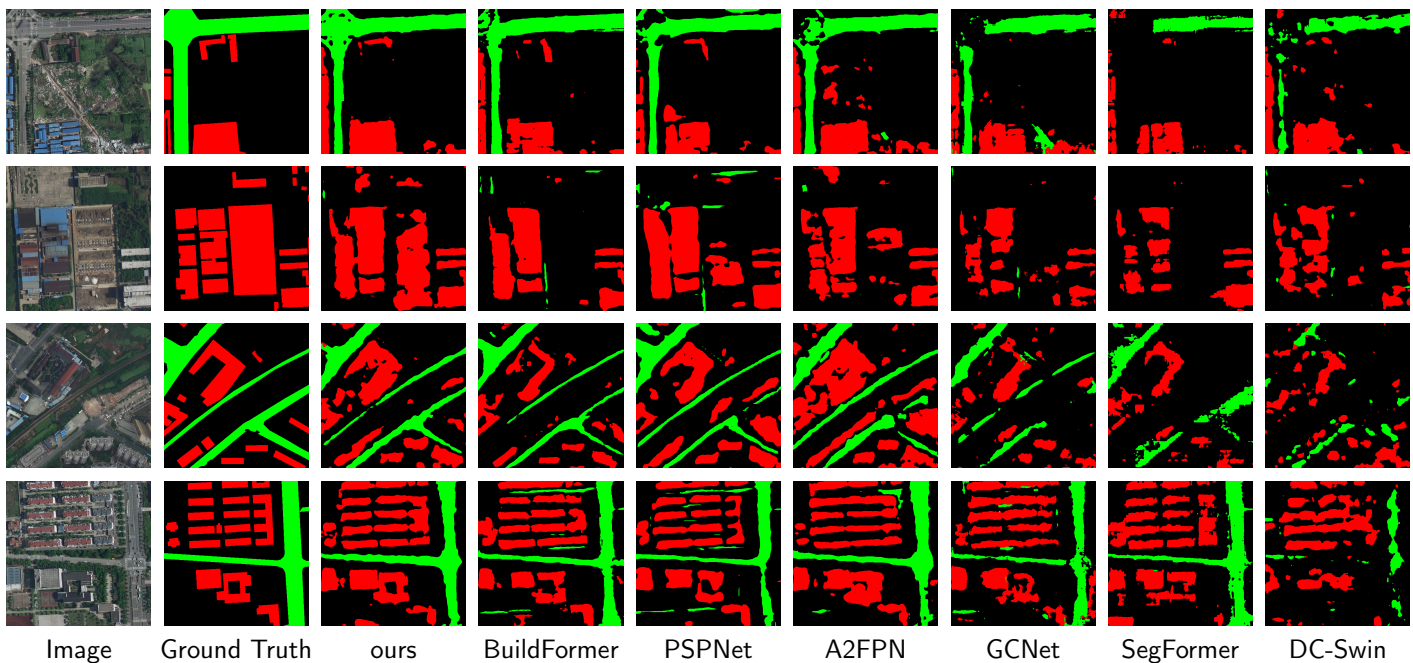
**Figure 5.** Experimental results on the private dataset.

4.5. Experimental results on the public dataset LoveDA

In this section, the compared experiments are conducted on LoveDA dataset. The compared models are the same as subsection. The comparison results are shown in Table 2 and Fig. 6. The proposed model outperforms the other compared models in both quantitative and qualitative results on the LoveDA dataset. The mIoU of LEDCNet is 1.22% higher than the powerful BuildFormer. And the IoU of the background and buildinghouses increased by 0.71% and 4.04% respectively compared with BuildFormer. The IoU of the road is slightly lower than that of BuildFormer. Furthermore, the overall accuracy and mean F1 score of the proposed model are 0.45% and 0.97% higher than the powerful BuildFormer. The performance of the large version of LEDCNet is slightly lower than that of the basic version. The performance of LDCNet as a backbone network surpasses ResNet18. It can be seen from the Fig. 6. That the proposed model extracts the whole building house area much better than other methods. And it extracts small roads better than most other methods. The proposed model has good detail extraction ability.

Table 2. Experimental results on the public dataset LoveDA.

Method	Backbone	Background (%)	building (%)	road (%)	OA (%)	mean F1 (%)	mIoU (%)
DC-Swin	-	88.41	32.94	24.34	92.47	60.85	48.57
SegFormer	-	90.85	36.00	33.89	93.60	66.10	53.31
GCNet	ResNet18	89.83	37.02	35.04	93.56	66.85	53.90
A2FPN	ResNet18	90.18	38.82	43.59	93.82	70.49	57.59
PSPNet	ResNet18	91.07	48.55	44.05	94.81	74.05	61.43
BuildFormer	-	91.94	49.97	50.26	94.97	76.44	64.05
LEDCNet (ours)	ResNet18	91.47	44.98	47.49	94.66	74.00	61.35
LEDCNet (ours)	LDCNet (ours)	92.65	54.01	<u>49.13</u>	95.42	77.41	65.27
LEDCNet-Large (ours)	LDCNet-Large (ours)	<u>92.59</u>	<u>52.89</u>	48.87	<u>95.39</u>	<u>77.00</u>	<u>64.79</u>

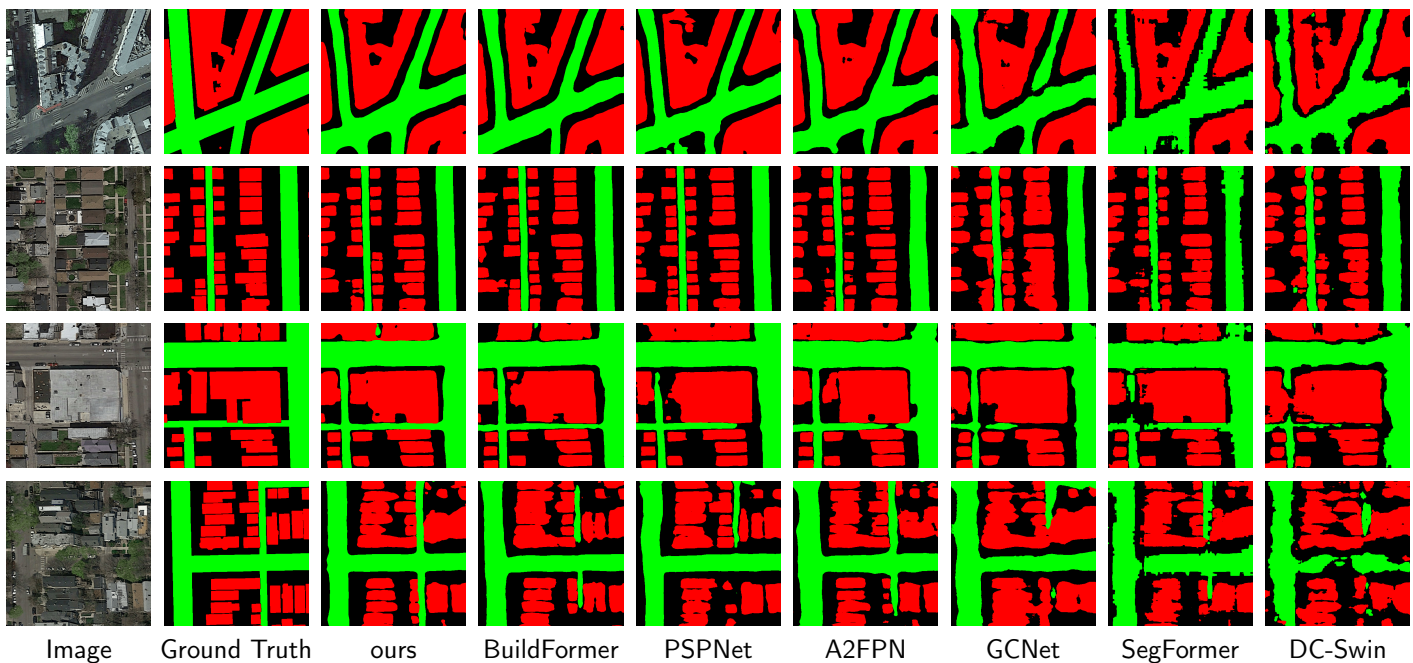
**Figure 6.** Experimental results on the public dataset LoveDA.

4.6. Experimental results on the public dataset CITY-OSM

In this section, a large-scale data set named CITY-OSM is used to demonstrate the performance of the proposed LEDCNet. From Table 3, On such our basic model performs slightly worse than the two models of PSPNet and BuildFormer. This demonstrates the good generalization ability of our basic model on smaller datasets. However, the large version of LEDCNet outperforms other methods. The mIoU is 0.28% higher than that of the powerful BuildFormer, and the IoU of buildinghouses and roads are 0.21% and 0.51% higher, respectively. It is obvious from Fig. 7. that the proposed model has strong road extraction ability.

Table 3. Experimental results on the public dataset CITY-OSM

Method	Backbone	Background (%)	building (%)	road (%)	OA (%)	mean F1 (%)	mIoU (%)
DC-Swin	-	63.71	68.79	55.06	85.42	76.79	62.52
SegFormer	-	67.35	72.69	61.73	87.48	80.34	67.26
GCNet	ResNet18	66.67	71.76	63.44	87.32	80.39	67.28
A2FPN	ResNet18	71.12	75.72	77.65	89.26	83.34	71.50
PSPNet	ResNet18	75.40	79.01	73.10	91.06	86.24	76.04
BuildFormer	-	75.36	79.30	72.79	91.08	86.22	75.82
LEDCNet (ours)	ResNet18	73.17	76.54	70.76	90.04	84.70	73.49
LEDCNet (ours)	LDCNet (ours)	73.95	78.25	70.95	90.49	85.28	74.39
LEDCNet-Large (ours)	LDCNet-large (ours)	75.51	79.51	73.30	91.17	86.41	76.10

**Figure 7.** Experimental results on the public dataset CITY_OSM.

4.7. Evaluation of Model Efficiency

It can be seen from the table 4 that the proposed model, whether it is the basic version or the enlarged version, has smaller parameters and model sizes than other models. In addition, the FLOPs of the proposed basic version of the model is also the smallest. Therefore, the proposed model can be applied in a variety of hardware performance-limited scenarios. However, the proposed model still has shortcomings, that is, the FPS is not the highest, which is what we need to improve in the next step.

Table 4. Evaluation of Model Efficiency

Method	Params (M)	Size (MB)	FLOPs (G)	FPS
DC-Swin	118	237.858	126.15	34.7
SegFormer	7.7	15.436	13.11	115.2
GCNet	61.5	122.933	9.84	182.6
A2FPN	12.2	24.318	13.21	201.4
PSPNet	24.3	48.648	96.53	98.5
BuildFormer	40.5	81.038	116.22	52.4
LEDCNet (ours)	1.4	2.628	5.48	212.6
LEDCNet-large (ours)	<u>6.1</u>	<u>12.271</u>	13.69	108.4

4.8. Ablation study

To evaluate the contribution of each component of the proposed LEDCNet the ablation experiments are conducted using LoveDA dataset and CITY_OSM dataset, as shown in Table 5. After adding the ASPP module to the baseline model, mIoU on the two public datasets increased by 0.55% and 0.42%, respectively. After adding the OCR module to the baseline model, mIoU on the two public datasets increased by 1.55% and 0.88%, respectively. After the proposed model aggregates these two modules, mIoU on two public datasets improves by 2.03% and 0.69% compared to the baseline model, respectively.

Table 5. Ablation study

Dataset	Method	Overall Accuracy	Mean F1-Score	mIoU
LoveDA	Baseline	94.79	75.77	63.24
	Baseline + ASPP	95.21	76.14	63.79
	Baseline + OCR	95.29	77.02	64.79
	Baseline + ASPP + OCR	95.42	77.41	65.27
CITY_OSM	Baseline	90.19	84.82	73.70
	Baseline + ASPP	90.36	85.11	74.12
	Baseline + OCR	90.32	85.03	74.00
	Baseline + ASPP + OCR	90.49	85.28	74.39

In addition, we also studied the impact of using different backbone networks on the performance of the model. As shown in Table 6, the proposed LDCNet surpasses mainstream backbone networks. Compared to ResNet18, the proposed method showed an improvement of 3.29% and 0.9% in mIoU on two common datasets, respectively.

Table 6. Comparison using different backbones.

Dataset	Method	Backbone	Mean F1-Score	mIoU
LoveDA	ResNet18	94.66	74.02	61.35
	DenseNet121	95.16	76.25	63.81
	Swin Transformer	95.08	75.98	63.55
	MobileNetV3	94.78	74.22	61.62
	LDCNet (ours)	95.42	77.41	65.27
CITY_OSM	ResNet18	90.04	84.70	73.49
	DenseNet121	90.38	85.14	74.32
	Swin Transformer	90.29	85.03	74.19
	MobileNetV3	89.91	84.37	73.01
	LDCNet (ours)	90.49	85.28	74.39

5. Discussion

LEDCNet has achieved excellent performance with a smaller number of parameters and lower computational cost. Compared to larger models in the past, it is suitable for running on a wider range of hardware conditions. There are three main reasons for the outstanding performance of the proposed model. Firstly, this paper customizes a lightweight and efficient backbone network LDCNet for LEDCNet, which extensively uses depthwise separable convolutions and some design techniques. This makes LDCNet both computationally efficient and powerful in feature extraction. Secondly, LEDCNet has two contextual feature extraction modules. The ASPP module can obtain features of different scales of buildings or roads in remote sensing images by using different sizes of receptive fields, while the OCR module can focus more on the relationships between pixels within a single category of buildings or roads, which is of great help in edge extraction. Therefore, these two modules complement each other. In addition, FPN combines semantic features of different levels, enhancing the network's ability to extract small-scale targets.

6. Conclusions

In this paper, a lightweight and efficient semantic segmentation network based on encoder-decoder structure was developed for buildings and roads extraction from UAV remote sensing images. The encoder used a new lightweight and high-performance backbone network proposed in this paper to accelerate model calculation and reduce model parameters. The decoder employed a dual-context module combined with ASPP and OCR to effectively capture multi-scale contextual information. Extensive experiments demonstrate that the proposed model achieved high performance on both private and two public datasets, with fewer parameters and operations. In the future, we hope that our LEDCNet can be expanded to more semantic segmentation fields. We will continue to improve this model to make it more efficient.

Author Contributions: Methodology, X.Han. and Y.Liu.; Software, X.Han. and Y.Liu.; Visualization, Y.Lin. and G.Liu.; Writing—original draft, X.Han. and Y.Liu.; Writing—review & editing, G.Liu. and Q.Liu.

Funding: This research was partially supported by the National Natural Science Foundation of China (Project No. 61801288).

Conflicts of Interest: The authors declare no conflict of interest.

References

1. Osco, L.P.; Junior, J.M.; Ramos, A.P.M.; de Castro Jorge, L.A.; Fatholahi, S.N.; de Andrade Silva, J.; Matsubara, E.T.; Pistori, H.; Gonçalves, W.N.; Li, J. A review on deep learning in UAV remote sensing. *International Journal of Applied Earth Observation and Geoinformation* **2021**, *102*, 102456.

2. Long, J.; Shelhamer, E.; Darrell, T. Fully convolutional networks for semantic segmentation. In Proceedings of the Proceedings of the IEEE conference on computer vision and pattern recognition, 2015, pp. 3431–3440.
3. Badrinarayanan, V.; Kendall, A.; Cipolla, R. Segnet: A deep convolutional encoder-decoder architecture for image segmentation. *IEEE transactions on pattern analysis and machine intelligence* **2017**, *39*, 2481–2495.
4. Ronneberger, O.; Fischer, P.; Brox, T. U-net: Convolutional networks for biomedical image segmentation. In Proceedings of the International Conference on Medical image computing and computer-assisted intervention. Springer, 2015, pp. 234–241.
5. Zhao, H.; Shi, J.; Qi, X.; Wang, X.; Jia, J. Pyramid scene parsing network. In Proceedings of the Proceedings of the IEEE conference on computer vision and pattern recognition, 2017, pp. 2881–2890.
6. Chen, L.C.; Papandreou, G.; Kokkinos, I.; Murphy, K.; Yuille, A.L. Semantic image segmentation with deep convolutional nets and fully connected crfs. *arXiv preprint arXiv:1412.7062* **2014**.
7. Chen, L.C.; Papandreou, G.; Kokkinos, I.; Murphy, K.; Yuille, A.L. Deeplab: Semantic image segmentation with deep convolutional nets, atrous convolution, and fully connected crfs. *IEEE transactions on pattern analysis and machine intelligence* **2017**, *40*, 834–848.
8. Chen, L.C.; Papandreou, G.; Schroff, F.; Adam, H. Rethinking atrous convolution for semantic image segmentation. *arXiv preprint arXiv:1706.05587* **2017**.
9. Chen, L.C.; Zhu, Y.; Papandreou, G.; Schroff, F.; Adam, H. Encoder-decoder with atrous separable convolution for semantic image segmentation. In Proceedings of the Proceedings of the European conference on computer vision (ECCV), 2018, pp. 801–818.
10. Liu, W.; Yang, M.; Xie, M.; Guo, Z.; Li, E.; Zhang, L.; Pei, T.; Wang, D. Accurate building extraction from fused DSM and UAV images using a chain fully convolutional neural network. *Remote Sensing* **2019**, *11*, 2912.
11. Hossain, M.D.; Chen, D. A hybrid image segmentation method for building extraction from high-resolution RGB images. *ISPRS Journal of Photogrammetry and Remote Sensing* **2022**, *192*, 299–314.
12. Sultonov, F.; Park, J.H.; Yun, S.; Lim, D.W.; Kang, J.M. Mixer U-Net: An improved automatic road extraction from UAV imagery. *Applied Sciences* **2022**, *12*, 1953.
13. Guan, H.; Lei, X.; Yu, Y.; Zhao, H.; Peng, D.; Junior, J.M.; Li, J. Road marking extraction in UAV imagery using attentive capsule feature pyramid network. *International Journal of Applied Earth Observation and Geoinformation* **2022**, *107*, 102677.
14. Huang, G.; Liu, Z.; Van Der Maaten, L.; Weinberger, K.Q. Densely connected convolutional networks. In Proceedings of the Proceedings of the IEEE conference on computer vision and pattern recognition, 2017, pp. 4700–4708.
15. Liu, Z.; Mao, H.; Wu, C.Y.; Feichtenhofer, C.; Darrell, T.; Xie, S. A convnet for the 2020s. In Proceedings of the Proceedings of the IEEE/CVF Conference on Computer Vision and Pattern Recognition, 2022, pp. 11976–11986.
16. Liu, Z.; Lin, Y.; Cao, Y.; Hu, H.; Wei, Y.; Zhang, Z.; Lin, S.; Guo, B. Swin transformer: Hierarchical vision transformer using shifted windows. In Proceedings of the Proceedings of the IEEE/CVF International Conference on Computer Vision, 2021, pp. 10012–10022.
17. He, K.; Zhang, X.; Ren, S.; Sun, J. Deep residual learning for image recognition. In Proceedings of the Proceedings of the IEEE conference on computer vision and pattern recognition, 2016, pp. 770–778.
18. Yuan, Y.; Chen, X.; Chen, X.; Wang, J. Segmentation transformer: Object-contextual representations for semantic segmentation. *arXiv preprint arXiv:1909.11065* **2019**.
19. Lin, T.Y.; Dollár, P.; Girshick, R.; He, K.; Hariharan, B.; Belongie, S. Feature pyramid networks for object detection. In Proceedings of the Proceedings of the IEEE conference on computer vision and pattern recognition, 2017, pp. 2117–2125.
20. Maggiori, E.; Tarabalka, Y.; Charpiat, G.; Alliez, P. Convolutional neural networks for large-scale remote-sensing image classification. *IEEE Transactions on geoscience and remote sensing* **2016**, *55*, 645–657.
21. Liu, Y.; Minh Nguyen, D.; Deligiannis, N.; Ding, W.; Munteanu, A. Hourglass-shapenetwork based semantic segmentation for high resolution aerial imagery. *Remote Sensing* **2017**, *9*, 522.
22. Fu, G.; Liu, C.; Zhou, R.; Sun, T.; Zhang, Q. Classification for high resolution remote sensing imagery using a fully convolutional network. *Remote Sensing* **2017**, *9*, 498.
23. Li, R.; Liu, W.; Yang, L.; Sun, S.; Hu, W.; Zhang, F.; Li, W. DeepUNet: A deep fully convolutional network for pixel-level sea-land segmentation. *IEEE Journal of Selected Topics in Applied Earth Observations and Remote Sensing* **2018**, *11*, 3954–3962.
24. Cheng, B.; Liang, C.; Liu, X.; Liu, Y.; Ma, X.; Wang, G. Research on a novel extraction method using Deep Learning based on GF-2 images for aquaculture areas. *International Journal of Remote Sensing* **2020**, *41*, 3575–3591.
25. Wang, Y.; Peng, Y.; Li, W.; Alexandropoulos, G.C.; Yu, J.; Ge, D.; Xiang, W. DDU-Net: dual-decoder-U-Net for road extraction using high-resolution remote sensing images. *IEEE Transactions on Geoscience and Remote Sensing* **2022**, *60*, 1–12.
26. Song, S.; Liu, J.; Liu, Y.; Feng, G.; Han, H.; Yao, Y.; Du, M. Intelligent object recognition of urban water bodies based on deep learning for multi-temporal and multi-temporal high spatial resolution remote sensing imagery. *Sensors* **2020**, *20*, 397.
27. Weng, L.; Xu, Y.; Xia, M.; Zhang, Y.; Liu, J.; Xu, Y. Water areas segmentation from remote sensing images using a separable residual segnet network. *ISPRS International Journal of Geo-Information* **2020**, *9*, 256.
28. Kniaz, V.V. Deep learning for dense labeling of hydrographic regions in very high resolution imagery. In Proceedings of the Image and signal processing for remote sensing XXV. SPIE, 2019, Vol. 11155, pp. 283–292.

29. Goodfellow, I.; Pouget-Abadie, J.; Mirza, M.; Xu, B.; Warde-Farley, D.; Ozair, S.; Courville, A.; Bengio, Y. Generative adversarial networks. *Communications of the ACM* **2020**, *63*, 139–144.
30. Wang, Q.; Huang, H.; Zhong, Y.; Min, W.; Han, Q.; Xu, D.; Xu, C. Swin Transformer Based on Two-Fold Loss and Background Adaptation Re-Ranking for Person Re-Identification. *Electronics* **2022**, *11*, 1941.
31. Li, R.; Zheng, S.; Zhang, C.; Duan, C.; Su, J.; Wang, L.; Atkinson, P.M. Multiattention network for semantic segmentation of fine-resolution remote sensing images. *IEEE Transactions on Geoscience and Remote Sensing* **2021**, *60*, 1–13.
32. Zhang, C.; Jiang, W.; Zhang, Y.; Wang, W.; Zhao, Q.; Wang, C. Transformer and CNN Hybrid Deep Neural Network for Semantic Segmentation of Very-High-Resolution Remote Sensing Imagery. *IEEE Transactions on Geoscience and Remote Sensing* **2022**, *60*, 1–20.
33. Howard, A.G.; Zhu, M.; Chen, B.; Kalenichenko, D.; Wang, W.; Weyand, T.; Andreetto, M.; Adam, H. Mobilenets: Efficient convolutional neural networks for mobile vision applications. *arXiv preprint arXiv:1704.04861* **2017**.
34. Sandler, M.; Howard, A.; Zhu, M.; Zhmoginov, A.; Chen, L.C. Mobilenetv2: Inverted residuals and linear bottlenecks. In Proceedings of the Proceedings of the IEEE conference on computer vision and pattern recognition, 2018, pp. 4510–4520.
35. Howard, A.; Sandler, M.; Chu, G.; Chen, L.C.; Chen, B.; Tan, M.; Wang, W.; Zhu, Y.; Pang, R.; Vasudevan, V.; et al. Searching for mobilenetv3. In Proceedings of the Proceedings of the IEEE/CVF international conference on computer vision, 2019, pp. 1314–1324.
36. Iandola, F.N.; Han, S.; Moskewicz, M.W.; Ashraf, K.; Dally, W.J.; Keutzer, K. SqueezeNet: AlexNet-level accuracy with 50x fewer parameters and < 0.5 MB model size. *arXiv preprint arXiv:1602.07360* **2016**.
37. Tan, M.; Le, Q. Efficientnet: Rethinking model scaling for convolutional neural networks. In Proceedings of the International conference on machine learning. PMLR, 2019, pp. 6105–6114.
38. Han, K.; Wang, Y.; Tian, Q.; Guo, J.; Xu, C.; Xu, C. Ghostnet: More features from cheap operations. In Proceedings of the Proceedings of the IEEE/CVF conference on computer vision and pattern recognition, 2020, pp. 1580–1589.
39. Li, Y.; Chen, Y.; Dai, X.; Chen, D.; Liu, M.; Yuan, L.; Liu, Z.; Zhang, L.; Vasconcelos, N. Micronet: Improving image recognition with extremely low flops. In Proceedings of the Proceedings of the IEEE/CVF International Conference on Computer Vision, 2021, pp. 468–477.
40. Cao, Y.; Xu, J.; Lin, S.; Wei, F.; Hu, H. Gcnet: Non-local networks meet squeeze-excitation networks and beyond. In Proceedings of the Proceedings of the IEEE/CVF international conference on computer vision workshops, 2019, pp. 0–0.
41. Peng, C.; Zhang, X.; Yu, G.; Luo, G.; Sun, J. Large kernel matters—improve semantic segmentation by global convolutional network. In Proceedings of the Proceedings of the IEEE conference on computer vision and pattern recognition, 2017, pp. 4353–4361.
42. Xie, S.; Girshick, R.; Dollár, P.; Tu, Z.; He, K. Aggregated residual transformations for deep neural networks. In Proceedings of the Proceedings of the IEEE conference on computer vision and pattern recognition, 2017, pp. 1492–1500.
43. Szegedy, C.; Liu, W.; Jia, Y.; Sermanet, P.; Reed, S.; Anguelov, D.; Erhan, D.; Vanhoucke, V.; Rabinovich, A. Going deeper with convolutions. In Proceedings of the Proceedings of the IEEE conference on computer vision and pattern recognition, 2015, pp. 1–9.
44. Ding, X.; Zhang, X.; Han, J.; Ding, G. Scaling up your kernels to 31x31: Revisiting large kernel design in cnns. In Proceedings of the Proceedings of the IEEE/CVF Conference on Computer Vision and Pattern Recognition, 2022, pp. 11963–11975.
45. Guo, M.H.; Lu, C.Z.; Liu, Z.N.; Cheng, M.M.; Hu, S.M. Visual attention network. *arXiv preprint arXiv:2202.09741* **2022**.
46. Ioffe, S. Batch renormalization: Towards reducing minibatch dependence in batch-normalized models. *Advances in neural information processing systems* **2017**, *30*.
47. Wu, Y.; Johnson, J. Rethinking" batch" in batchnorm. *arXiv preprint arXiv:2105.07576* **2021**.
48. Ba, J.L.; Kiros, J.R.; Hinton, G.E. Layer normalization. *arXiv preprint arXiv:1607.06450* **2016**.
49. Wang, J.; Zheng, Z.; Ma, A.; Lu, X.; Zhong, Y. LoveDA: A remote sensing land-cover dataset for domain adaptive semantic segmentation. *arXiv preprint arXiv:2110.08733* **2021**.
50. Kaiser, P.; Wegner, J.D.; Lucchi, A.; Jaggi, M.; Hofmann, T.; Schindler, K. Learning aerial image segmentation from online maps. *IEEE Transactions on Geoscience and Remote Sensing* **2017**, *55*, 6054–6068.
51. Loshchilov, I.; Hutter, F. Fixing weight decay regularization in adam **2018**.
52. Lin, T.Y.; Goyal, P.; Girshick, R.; He, K.; Dollár, P. Focal loss for dense object detection. In Proceedings of the Proceedings of the IEEE international conference on computer vision, 2017, pp. 2980–2988.
53. Xie, E.; Wang, W.; Yu, Z.; Anandkumar, A.; Alvarez, J.M.; Luo, P. SegFormer: Simple and efficient design for semantic segmentation with transformers. *Advances in Neural Information Processing Systems* **2021**, *34*, 12077–12090.
54. Li, R.; Wang, L.; Zhang, C.; Duan, C.; Zheng, S. A2-FPN for semantic segmentation of fine-resolution remotely sensed images. *International journal of remote sensing* **2022**, *43*, 1131–1155.
55. Wang, L.; Li, R.; Duan, C.; Zhang, C.; Meng, X.; Fang, S. A novel transformer based semantic segmentation scheme for fine-resolution remote sensing images. *IEEE Geoscience and Remote Sensing Letters* **2022**, *19*, 1–5.
56. Wang, L.; Fang, S.; Meng, X.; Li, R. Building extraction with vision transformer. *IEEE Transactions on Geoscience and Remote Sensing* **2022**, *60*, 1–11.

Disclaimer/Publisher's Note: The statements, opinions and data contained in all publications are solely those of the individual author(s) and contributor(s) and not of MDPI and/or the editor(s). MDPI and/or the editor(s) disclaim responsibility for any injury to people or property resulting from any ideas, methods, instructions or products referred to in the content.